

BRIDGE MAINTENANCE ROBOTIC ARM: CAPACITIVE SENSOR FOR OBSTACLE RANGING IN PARTICLE LADEN AIR

Nathan Kirchner, Dikai Liu and Gamini Dissanayake

Centre for Autonomous Systems

Kevin Kirby Suite, Building 2, Level 6

University of Technology, Sydney

Broadway 2007, NSW. Australia

n.kirchner@cas.edu.au, d.liu@cas.edu.au and g.dissanayake@cas.edu.au

Abstract: This paper describes an Adaptive Capacitive Sensor Network for Obstacle Ranging (ACSOR) that is intended to provide entire arm encompassing obstacle range data for a robotic arm conducting the task of sandblasting a bridge. A multi-channel capacitive sensor capable of dynamic obstacle ranging in air heavily laden with lead contaminated sandblasting refuse has been developed. Experimental results have shown the ACSOR's working range to be 50cm, that it is relatively immune from airborne lead contaminated sandblasting refuse and that it is capable of ranging an obstacle 21cm away whilst fitted to a robotic arm moving at 2cm/s with an obstacle range error of less than 1cm.

Keywords: Capacitive, range sensor, obstacle avoidance, harsh environment

1. INTRODUCTION

Bridges are essential in transport infrastructure worldwide and with their high construction costs there is significant motivation to extend their life spans. Research into premature failure has identified rust as a primary cause, [1] and [2], and stripping the structure back to clean, untainted metal and then applying a paint coating as a means of effective protection. The most effective method of large scale metal stripping such as that necessary for a bridge is sandblasting, and herein lies the problem. Sandblasting is a labor intensive and hazardous [3] operation. Not only do workers have to spend long periods of time handling up to 400N forces [4], but a large portion of bridges in Australia, including the Sydney Harbour Bridge, are painted with lead and/or asbestos based paints. These types of paint pose a serious health risk to workers tasked with their removal. With the long-term health damage done by lead and asbestos being now commonly known [5] the appeal of replacing manual labor with robotic labor is high. This, along with changing workplace laws, which are slowly evolving to prohibit humans from working in such environments, leave little alternative other than robotics in order to complete this necessary task.

Typical sandblasting environments have fluctuating light, extreme full spectrum white noise, airborne lead/sand particles, airborne paint flakes and are dynamic; complete mapping of the environment in order to identify all obstacles that must be avoided is extremely difficult [6] and thus the operating environment is often only partially known. With the operating environment partially unknown effective collision avoidance cannot rely solely on a map but will require some form of active obstacle range sensing [7] that can encompass the entire robot, such as Cheung's, et al. (1989) infrared based "Sensitive Skin" [8] or Vranish's, et al. (1990) mechanical "Collision Avoidance Skin" [9]. Since

infrared will be defeated in typical sandblasting environments (discussed later) and as contact sensing is not desirable, developing a sensor network "skin" that can function in this environment is the first step towards the overall goal of developing a robotic system capable of sandblasting.

There are several mature sensors available for obstacle ranging applications. With the sensors falling into the categories of Laser, Ultrasonic, InfraRed (IR), Radio Frequency (RF), Visual and Capacitive. However due to the nature of typical sandblasting environments these sensors are likely to be ineffective. The laser is dispersed by the airborne particles [10]; these particles also affect the ultrasonic, RF and IR in a similar manner and impair the vision sensor [11 and references within] rendering them unusable. Ultrasonic is further impaired by the white noise, as is IR by the presence of natural light.

Capacitive-based proximity sensing offers many advantages. The broad distribution of the electric field allows large areas of coverage with a small number of sensors. Additionally, capacitive sensors are insensitive to lighting, noise, or the color, shape, surface and texture of the obstacle [12]. Although many manufactures offer capacitive sensors designed for short distances (<1cm) [13] and current research is tending towards very short range capacitive sensors (<2000μm) [15] this is not indicative of the technologies capabilities as demonstrated by Novak, et al. (1992) who developed a capacitive sensor with a range of 40cm [12] and successfully demonstrated obstacle avoidance with the sensor fitted to an anthropomorphic robotic arm [15]. Airborne lead/sand will affect the accuracy of the sensor, but the effect is unlikely to be as detrimental as with the pre-mentioned sensors. Even so, no work has been done to adapt the capacitive sensors to the type of environments typical in sandblasting operations or to implement them into a sensor network, "skin".

This paper presents the Adaptive Capacitive Sensor for Object Ranging (ACSOR). The ACSOR is an extension of the sensor developed by Novak, et al. in 1992 [12] that has adapted Novak's sensor to allow operation in air heavily laden with lead contaminated sandblasting refuse. The ACSOR has also extended the sensing range from 40cm to 50cm. The ACSOR has been fitted to an anthropomorphic robotic arm and demonstrated the ability to measure the range to an object at 21cm within 1cm accuracy while the arm was in motion at 2cm/s.

The breakdown of this paper is as follows; firstly the fundamentals of the ACSOR will be discussed followed by a discussion of the modifications that differentiate the ACSOR. Section 4 will detail the results from ACSOR testing, these results will then be discussed with conclusions drawn and future work proposed.

2. FUNDAMENTALS

Figure 1 shows a schematic of the active sensing component of the ACSOR. The ACSOR is built on the same fundamental technology as Novak's sensor and the reader is referred to [12] for an in-depth explanation. In this paper only conductive obstacles will be considered as the intended application is for sensing bridge structures. The obstacles are assumed to be flat plates orientated parallel to the sensor. This assumption is reasonable considering the size of the sensor (7cm x 7cm) compared to the size of the intended object being sensed.

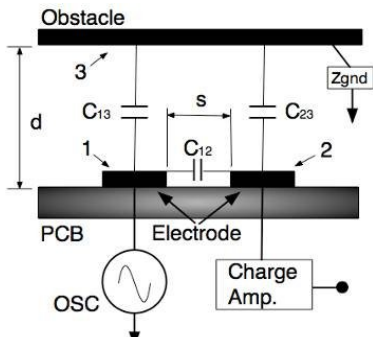


Figure 1 Schematic of active sensing component

Referring to Figure 1, electrode 1 is connected to a drive oscillator and electrode 2 is connected to a charge amplifier. As the magnitude of the electric field generated by the drive oscillator on electrode 1 is fixed and as electric fields will follow the path of least resistance then in the case where no obstacles are present the electric field tends to electrode 2 and give rise to a maximum charge, Q , between electrodes 1 and 2, shown in (1).

$$Q = \int_S \epsilon E dS \quad (1)$$

where E is the electric field vector and S is a surface completely enclosing the conductors. In the model shown in Figure 1 the surface S reduces to a continuous path around the conductor.

The charge, Q , is determined by the drive oscillator voltage and remains fixed whilst the drive oscillator voltage is fixed. In the case shown in Figure 1 where an obstacle with high impedance to ground is present Q becomes the sum of capacitances C_{12} , C_{23} and C_{13} and as Q is fixed and C_{23} and C_{13} are greater than zero, C_{12} must be of reduced magnitude (conservation of energy). Further to this, as capacitance is proportional to the distance between electrodes, the distance d is directly related to C_{23} and C_{13} and thus C_{12} . Due to the electrical configuration of the charge amplifier circuit the charge amplifier measures the sensor capacitance, C_{12} , only. It is this property of the sensor that is exploited to facilitate range measurements.

Figure 2 shows a schematic showing the effect of an airborne particle on the sensor. Electrode 1 is shown (the effect on electrode 2 will be identical) in two configurations. The first (left) is the case of no dust, as in Figure 1. The second (right) is in the case of several dust particles between the electrode and the obstacle.

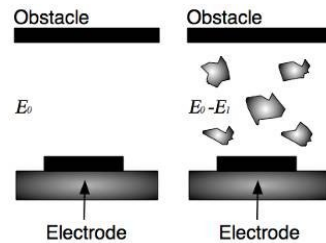


Figure 2 Schematic of effect of airborne particle

The introduction of the particles increases permittivity, ϵ , of the dielectric resulting in a reduced voltage and thus a reduced electric field between the plates (2). The electric field, E_0 , generated by the charge stored on the capacitor plates is partially canceled out by an opposing electric field, E_1 , generated by the polarization of the constituent molecules of the dielectric [16].

$$C = \frac{Q}{V} = \frac{\epsilon A}{d} \quad (2)$$

It follows that the strength of the opposing field E_1 is also proportional to E_0 . Using the constant of proportionality the net electric field between the plates can be expressed as shown in (3), where K is the dielectric constant. The equation shows that the electric field between the plates is reduced by a factor K with respect to the vacuum case.

$$E_0 - E_1 = \frac{E_0}{K} \quad (3)$$

Note that the degree of polarization of a polarizable molecule is proportional to the external electric field strength E_0 and breaks down if E_0 becomes large, meaning when E_0 is large, the effect of E_1 becomes negligible leaving the electric field unaffected by the particles.

3. ACSOR

As previously mentioned the ACSOR is built on the same fundamental technology as Novak's sensor, described in [12]. However significant changes have been made to improve the robustness, accuracy and range as well as the most distinguishing modification that allows the ACSOR operation in typical sandblasting environments.

Figure 3 shows a diagram of the ACSOR sensor, the figure highlights an immediate difference to Novak's sensor. The ACSOR uses two sets of electrodes, driven at different frequencies. This facilitates the use of more intelligent filtering techniques on the sensor output to reduce sensor noise. For instance, the electrodes when driven at different frequencies produce significantly different and complimentary transfers functions (detailed in Section 4) allowing improvements in accuracy, range and robustness via data fusion.

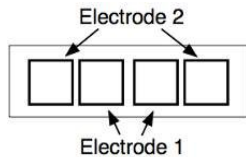


Figure 3 ACSOR Sensor

The ACSOR further differentiates itself from Novak's sensor via the changes made to drive and analysis circuitry that allow the ACSOR to run at a voltage approximately twice that of Novak's sensor. Although the electronic changes are not impressive in themselves the discovery that by running the sensor at a higher voltage the effect of the change of dielectric (from air to air/lead/sand) can approach zero, effectively allowing the sensor to operate immune to airborne lead and sand particles is a significant contribution to the technology.

Further modifications to the sensors operation have reduced the inter-sensor interference to allow for large sensor networks. A sensor network ideology (SNet) has been developed to connect multiple ACSORs together into a robust network to provide a larger or an all encompassing sensing zone. Whilst tentative results from this work have shown SNet's ability to self-organize, self-monitor and self-repair a network of ACSORs this work is not presented in this paper and will be published at a later date.

4. RESULTS

The ACSOR was evaluated through several different experiments in two different lab spaces. The first test was designed to determine the effect of drive frequency fluctuations on the sensor. The ACSOR was placed on the test bench with its sensing area facing upwards into empty space. The ACSOR was then calibrated to set the output to the full-scale deflection (FSD) of 900. The drive frequency was changed in three discrete steps, $\Delta 1\text{kHz}$, $\Delta 2\text{kHz}$ and $\Delta 5\text{kHz}$ from the original drive frequency with the effect on the output recorded for each instance. This test was repeated

for drive frequencies ranging from 50kHz to 200kHz. Figure 4 shows the results of this test.

It is important to mention at this stage that the output of the ACSOR is non-dimensional, the output can only be evaluated relative to itself. It is for this reason that the change in output is most often highlighted rather than the actual value of the output.

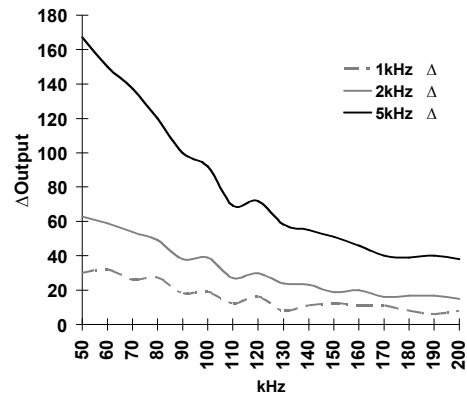


Figure 4 Effect of change in drive frequency

As can be seen from the figure the effect of drive frequency drift is significantly more profound with lower drive frequencies. With a drive frequency of 50kHz a $\Delta 5\text{kHz}$ drift causes a change of output equal to one-fifth of the FSD (170/900) of the sensor, conversely, with a drive frequency of 140kHz a $\Delta 5\text{kHz}$ drift causes a one-fifteenth of FSD (60/900) of the sensor change in the output reading. The variation in the effect of a drive frequency variation is not as significant when comparing a 140kHz drive frequency to a 200kHz one. This test reveals that significant robustness can be added to the ACSOR by insuring all drive frequencies are above 140kHz.

The next test was designed to determine the working range and transfer function of the ACSOR. Figure 5 shows the ACSORs configuration during the test; the test was conducted in a computer lab. The ACSOR was fixed to a grounded metal plate and another metal plate with high impedance to ground posing as the obstacle was placed parallel to the ACSOR. The obstacle was placed at various distances from the ACSOR, at 2cm increments, ranged from 2cm to 50cm. The range was limited to 50cm as this is the desired operating range of the sensor for the proposed application. The output readings were recorded during the entire duration of the test and the test was repeated numerous times and at two different drive frequencies, 159.8kHz and 169.2kHz, the results of the test are shown in Figure 6.

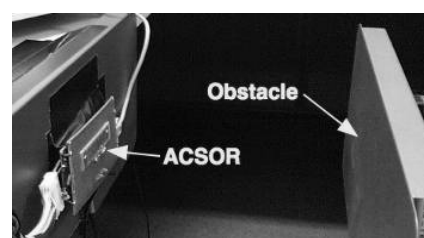


Figure 5 ACSOR range and transfer function testing

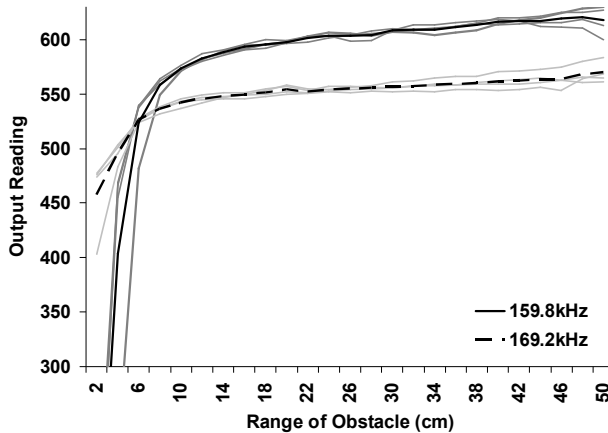


Figure 6 Results from range and transfer function test

As can be seen from the figure the two drive frequencies produced differing transfer functions, the 159.8kHz output reading dropped dramatically with the obstacle within 10cm unlike the 169.2kHz result. The two transfer functions also differ from the 10-50cm with the gradient of the 159.8kHz and 169.2kHz results being 1.15 and 0.675 respectively. Although this is an overly simplified comparison, as the two lines are not straight, it does serve to highlight that the functions are distinctively different. This result is very important as it suggests that the ACSOR would benefit from data fusion techniques. Another key result shown here is that the output readings are still discernable at 50cm showing that the sensor range is 50cm. The result also suggests that the sensor may be able to determine the range of obstacles beyond this.

The ACSOR's ability to function in air heavily laden with lead contaminated particles was then tested. Figure 7 shows the set-up for this test; this test was again conducted in the computers lab. The configuration is similar to that of the previous test however during this test lead contaminated refuse recovered from sandblasting operations at the Sydney Harbour Bridge was manually poured into the air gap between the ACSOR and obstacle at twice the mass flow rate (100g/s) typically used by sandblasters. The refuse was typical of bridge sandblasting, it was contaminated with lead and contained paint flakes and garnet of various sizes and shapes. The test was conducted at one obstacle-sensor spacing, 22cm and one drive frequency, 169.2kHz. The sensor was set to sample at 100Hz to limit the amount of data that needed to be stored; the sensor is capable of sampling at 50kHz.

The refuse used for this test was collected from post filtering. Filtering removes the fine lead particles that poison via inhalation and that pose the most significant health risk, and leaves only the heavy lead, which requires ingestion to be dangerous. The removal of the fine lead whilst significantly reducing the danger of using the refuse in the test only removed a small portion of the total mass of lead in the sample and its removal is not believed to have effected the results of the experiment.

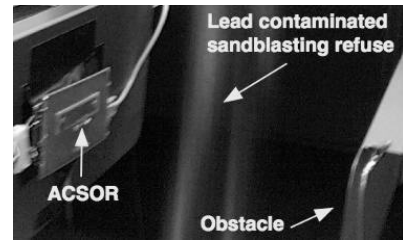


Figure 7 ACSOR effect of particle laden air test

Table 1 shows the results from this experiment, each of the ten tests contained ten one hundred sample sub-tests. The output reading is the average of the sub-tests and standard deviation is between each of the ten sub-tests. As can be seen from comparing the standard deviations from the clear and dusty tests the dusty tests display more deviation indicating that the dust introduces noise into the readings. Interestingly though, the overall average of both the clear and dusty tests are the same indicating that the noise introduced by the dust is zero mean. The overall standard deviation of the dusty test is 1.9 units larger than for the clear tests, this equates to a 3.5cm error rather than the 2.5cm error for the clear tests, (from Figure 6). Considering the intended application this is not significant.

Table 1 Results from particle laden air test

Test	Clear		Dusty	
	Output Reading	σ	Output Reading	σ
1	273	1.99	278	5.89
2	273	3.77	275	5.54
3	275	3.31	274	5.13
4	274	2.39	274	4.31
5	273	1.38	267	4.52
6	270	2.31	271	3.49
7	270	2.29	266	7.53
8	268	3.46	266	4.20
9	268	3.91	268	2.17
10	270	2.18	268	3.75
\bar{x}	271		271	
σ	2.41		4.31	

Following this test the ACSOR was taken to a robotics lab and was fitted to a Denso 6-DOF anthropomorphic robotic arm, as shown in Figure 8. A complex movement (described later) was then programmed into the robot and the robot was then set into motion with the ACSOR output readings recorded during the duration of the test. Due to the robotics lab being a clean room this test was conducted in clear air.

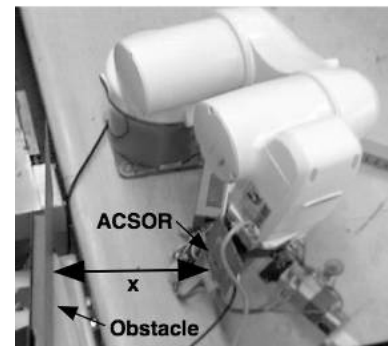


Figure 8 ACSOR fitted to robotic arm

The pre-mentioned complex movement program was written to command the robot to accelerate from stationary at $x = 31\text{cm}$ (with x shown in Figure 8) to $x = 28\text{cm}$ and then to move at 2cm/s until $x = 24\text{cm}$. Then to decelerate to be stationary at $x = 21\text{cm}$ and then accelerate back up to 2cm/s at $x = 18\text{cm}$. At 6cm from the obstacle the programmed commanded the robot to again decelerate to be stationary at $x = 3\text{cm}$ and to then move from $x = 3\text{cm}$ to $x = 31\text{cm}$ in one movement, with a similar acceleration profile as at $x = 3\text{-}6\text{cm}$ and $x = 28\text{-}31\text{cm}$. After this the program commanded the robot to move from $x = 3\text{cm}$ to $x = 31\text{cm}$ and then back to $x = 3\text{cm}$ in one movement again with a similar acceleration profile as at the end points. The entire process was repeated numerous times with the ACSOR being driven at 169.2kHz and with its readings being recorded for the duration of the test. The results are shown in Figure 9.

The first thing to note is that the sensitivity of the sensor is dramatically different compared to the previously shown results, Figure 6, with a movement from 10cm-30cm producing a 275 unit variation in the output reading where as when tested in the computer lab a movement over the same range produced a 25 unit variation. This is a significant difference, the cause of which is not known and will be investigated in future work.

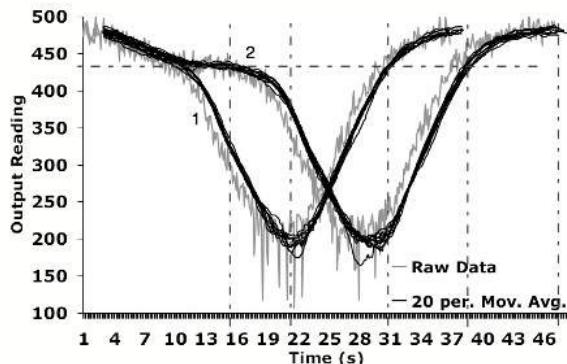


Figure 9 Results from robotic arm test

The grey lines in Figure 9 show the raw data from one of the numerous tests. As can be seen the sensor output is noisy, however the black lines, indicating 20-sample moving averages of the tests, sees a large amount of noise removed and a usable transfer function produced. The ACSOR was running at 10Hz to limit the amount of data to be stored, so in this case the moving window results in a 2 second lag in readings, running the sensor at a higher sample rate would significantly reduce this lag.

The results of Figure 9 clearly reflect the movement of the robot as previously described. The point of inflection at $t = 15$ corresponds to the momentary pause at $x = 21\text{cm}$. The output reading for curve 2 at $t = 15$ is 433. By using the known velocity profile and curve 1 from time 20 ($x = 3\text{cm}$) it is possible to calculate that the robot arm is 21cm from the obstacle at $t = 30$, the sensor output reading 435. By using the known velocity profile and curve 2 from time 48 ($x = 31\text{cm}$) and working backwards it is possible to calculate that the robot arm is 21cm from the obstacle at $t = 38.5$, the

sensor output reading 434. By comparing these calculations with the reading from the point of inflection it can be seen that the ACSOR can repeatability range the obstacle with $<1\text{cm}$ error, (at 21cm $\Delta 1\text{cm} \rightarrow \Delta 15$ units, derived from the figure and robot velocity of 2cm/s).

Figure 10 shows a portion of the results from the previously described test re-presented to show the transfer function of the sensor during this test. Figure 10 shows only the results from the portion of the overall arm movement described previously that consisted of the arm moving towards the obstacle, pausing at $x = 21\text{cm}$, moving again towards the obstacle to $x = 3\text{cm}$ and then moving away from the obstacle. The grey lines show the results from the numerous individual tests and the black line shows the average result over all of the tests. The x -axis of the graph corresponds to the distance x as defined in Figure 9.

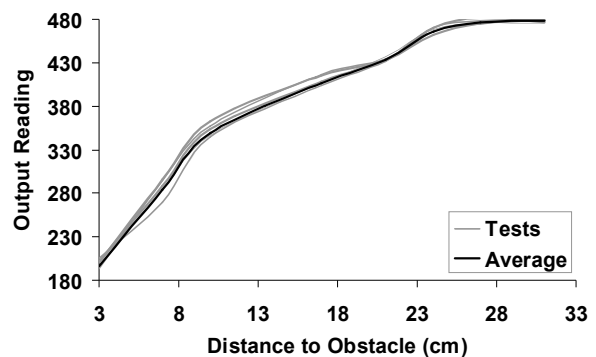


Figure 10 Results from robotic arm test

The first thing of note in this figure is that for the most part the results from the individual tests lie on the same line as each other and are indistinguishable. The separation that is most obvious at $x = 13\text{cm}$ is due to the output following one path when the ACSOR is moving towards the obstacle and another when the ACSOR is moving away from the obstacle. This result demonstrates that the ACSORs produces repeatable results, this is a significant result as repeatability is vital in sensors.

Also of note is that the output readings from the individual tests are closest to the overall average of all tests when the robotic arm is stationary. As can be seen at $x = 3\text{cm}$, $x = 21\text{cm}$ and $x = 31\text{cm}$ the results from the individual tests all converge to the average result showing significantly less result deviation. The cause of this is not known and will be investigated in future work but it is suspected that either vibration of the sensor due to movement of the arm or electrical noise from the robot's motors, when being driven, is the cause.

As can be seen from comparing the transfer function shown in this figure with the corresponding transfer function from Figure 6 the behavior of the sensor was dramatically different in the two labs. The transfer function from testing in the computer lab (Figure 6) shows the ACSOR to deliver an almost linear response from $x = 2\text{cm}$ to $x = 6\text{cm}$ with an output deviation of approximately 75 units. A hard 'knee' is then present at $x = 6\text{cm}$ to $x = 8\text{cm}$ after which the transfer is

again approximately linear up until $x = 31\text{cm}$ with an output variation of approximately 20 units.

The transfer function empirically derived from the testing in the robotics lab and shown in Figure 10 significantly differs from this with the response from $x = 2\text{cm}$ to $x = 31\text{cm}$ being a continuous curve with no obvious ‘knee’ or regions of linearity. The output variation for the range of greatest interest, $x = 8\text{cm}$ to $x = 31\text{cm}$, also significantly differs with a change in the output reading of approximately 200 units. As previously mentioned the cause of this discrepancy is not known and will be investigated in future work. Interference from 802.11g network in the computer lab is a possible cause.

5. CONCLUSIONS AND FUTURE WORK

This paper has presented the ACSOR which has been designed to be implemented into a sensor network in order to provide entire arm encompassing obstacle ranging in air heavily laden with lead and sand particles.

Experiments have demonstrated the ACSORs ability to range obstacles up to 50cm away. ACSORs relative immunity to air heavily laden with lead and sand particles have also been demonstrated with a less than 1cm effect on accuracy in the range measurements of an obstacle at 22cm. ACSORs ability to consistently and repeatedly range an obstacle at 21cm when fitted to a 6DOF anthropomorphic robotic arm moving at 2cm/s with less than 1cm error has also been shown. The evaluation of the ACSOR has demonstrated the sensors potential for use in our stated application and thus the technology will be pursued.

Future work will first investigate the variation in sensitivity of the ACSOR in the robotic lab compared to the computer lab. The increase of sensor output reading deviation from the average result when fitted to a robotic arm and during movement will also be investigated. Following this the SNet ideology will be implemented into an actual ACSOR sensor network.

ACKNOWLEDGMENTS

This work is supported by the ARC Centre of Excellence for Autonomous Systems (CAS), a UTS partnership grant with the Roads and Traffic Authority (RTA), the Australian Research Council (ARC) and the New South Wales State Government.

REFERENCES

- [1] Ferguson, P.J. “Painting metal bridges – Historical and current trends.” *J. Oil and Color Chemists' Assn.*, 59(7), 253, Middlesex, U.K. (1976)
- [2] Hare, C.H. “Protective coatings for bridge steel.” *Synthesis of Hwy. Pract.* 136, Transport Research Board, National Research Council, Washington, D.C. (1987)

- [3] Davies, B., “Remediating hazardous waste robotically using a high-level control systems and real-time sensors”, *Proc. Int. Symp. On Optical Tools for MFtg. and Advance Automation Telemanipulator Technology Conference*, Boston, MA, September (1993)
- [4] De Joode, B., Verspuy C. and Burdorf, A., “Physical workload in ship maintenance: Using The Observer to solve ergonomics problems”, *Noldus Information Technology – Erasmus University of Rotterdam*, Rotterdam, Netherlands. (2004)
- [5] HSE Information Services, “LEAD and You”, *HSE Books, ISBN 0 7176 1523 5*, Caerphilly, U.K. (1998)
- [6] Hhnel, D., Triebel, R., Burgard, W., and Thrun, S., “Map building with mobile robots in dynamic environments.” *Proc. of Int. Conf. on Robotics and Automation* (2003)
- [7] Chakravarthy, A., Debasish, G., “Obstacle Avoidance in Dynamic Environment: A Collision Cone Approach”, *IEEE Transactions on Systems, Man. and Cybernetic —Part A: Systems and Humans*, Vol.28, No. 5, Sept. (1998)
- [8] Cheung, E., Lumelsky, V., “Development of a Sensitive Skin for a 3D Robotic Arm Operating in an Uncertain Environment”, *Proc. of Int. Conf. on Robotics and Automation*, pp.1056-1061, Scottsdale, AZ, May (1989)
- [9] Vrannish, V., Chauhan, D., “Tri-mode collision avoidance skin for robot arm in space”, *Proc. of the Third Int. Symp. On Robotics and Manufacturing: Research, Education and Applications*, pp.189-195, Burnaby, Canada, July (1990)
- [10] Narihara, K., Toi, K., Hamada, Y., “Observation of dust particles by a laser scattering method in the JIPPT-IIU tokamak” *IAEA IoP Elec. Journal of Nucl. Fusion*, 37 pp.1177-1182. (1997)
- [11] A. Stentz, et al., “Position Measurement for Automated Mining Machinery”, *Proc. of Int. Conf. on Field and Service Robotics*, pp.299-304. August, (1999)
- [12] Novak, J. and Feddema, J., “A capacitance-based proximity sensor for whole arm obstacle avoidance”, *Proc. of Int. Conf. on Robotics and Automation*, vol. 2, pp.1307-1314, Albuquerque, U.S.A, May (1992)
- [13] Volpe, R., Ivlev, R.. “A Survey and Experimental Evaluation of Proximity Sensors for Space Robotics.” *Proc. of Int. Conf. on Robotics & Automation*, San Diego, CA, May (1994)
- [14] Smith, P., Vallance, R. and Marsh, E., “Correcting capacitive displacement measurements in metrology applications with cylindrical artifacts”, *ASPE Journal of Precision Engineering*, vol. 29, no 3, pp.324-335, (2005)
- [15] Feddema, J., Novak, J., “Whole arm obstacle avoidance for teleoperated robots”, *Proc. of Int. Conf. on Robotics and Automation*, vol.4, pp.3303-3309, San Diego, CA, May (1994)
- [16] Binns, K., Lawrenson, P., “Analysis and Computation of Electric and Magnetic Field Problems”, *Pergamon Press*, New York (1973)